UC Santa Barbara

UC Santa Barbara Previously Published Works

Title

Synthesis of a Series of Ln(III) (Ln = La, Ce, Lu) Aryl Complexes and Analysis of Their Ln–L Bonding Using Multinuclear NMR Spectroscopy and DFT Calculations

Permalink

https://escholarship.org/uc/item/9m9969h2

Journal

Inorganic Chemistry, 65(26)

ISSN

0020-1669

Authors

Dickinson, Grant

Yu, Xiaojuan

Stennett, Cary R

et al.

Publication Date

2026-07-06

DOI

10.1021/acs.inorgchem.6c01853

Copyright Information

This work is made available under the terms of a Creative Commons Attribution-NonCommercial License, available at https://creativecommons.org/licenses/by-nc/4.0/

Peer reviewed

eScholarship.org Powered by the California Digital Library
University of California

Synthesis of a Series of Ln(III) (Ln = La, Ce, Lu) Aryl Complexes and Analysis of their Ln-L Bonding using Multinuclear NMR Spectroscopy and DFT Calculations

Grant Dickinson[a], Xiaojuan Yu[b], Cary R. Stennett[c], Guang Wu[a], Jochen Autschbach[b]*, Trevor W. Hayton[a]*

[a] *Department of Chemistry and Biochemistry, University of California Santa Barbara, Santa Barbara, CA 93106*

[b] *Department of Chemistry, University at Buffalo, State University of New York, Buffalo, NY 14260*

[c] *Department of Chemistry, University of California, Irvine, CA 92697*

Email: hayton@chem.ucsb.edu, jochena@buffalo.edu

Abstract

The reaction of $[LaI_3(THF)_4]$ or $[Ce(NO_3)_3(THF)_4]$ with 4 equiv of *in situ* generated LiFmes (FmesH = 1,3,5-$(CF_3)_3C_6H_3$) resulted in the formation of the novel homoleptic lanthanide-aryl complexes $[Li(THF)_2(Et_2O)_2][La(Fmes)_4]$ ([Li][**1**]) and $[Li(THF)_{3.5}(Et_2O)_{0.5}][Ce(Fmes)_4]$ ([Li][**2**]), respectively. Likewise, the reaction of $[Lu(NO_3)_3(THF)_3]$ with 4 equiv of *in situ* generated LiFmes resulted in the formation of $[Li(THF)_3][LuF(Fmes)_3]$ ([Li][**3**]). Complexes [Li][**2**] and [Li][**3**] were isolated as mixtures with unreacted LiFmes. Additionally, the reaction of $[Lu(NO_3)_3(THF)_3]$ with 4 equiv of *in situ* generated LiC_6Cl_5 and 3 equiv of DME resulted in formation of the homoleptic lutetium-aryl complex, $[Li(DME)_3][Lu(C_6Cl_5)_4]$ ([Li][**4**]). All four complexes were characterized by X-ray crystallography and multi-nuclear NMR spectroscopy. In the solid state all four complexes exhibit weak F/Cl→Ln dative interactions; however, these interactions do not apparently offer much stability, since all four complexes are quite thermally sensitive. DFT calculations reveal that the Ln-C_{ipso} and Lu-F bonds are modestly covalent, although the Lu-F bond exhibits less covalency than the Ln-C_{ipso} bonds. The calculations also indicate that the La-C_{ipso} bonds exhibit a small amount of 4f orbital participation, whereas the Lu-C_{ipso} bonds have (as expected) no 4f character. Despite this difference, the spin-orbit deshielding effects on the C_{ipso} ^{13}C chemical shifts are comparable between complexes $[\mathbf{1}]^-$ and $[\mathbf{3}]^-$.

Introduction

In comparison to metal-ligand bonding in the actinides or transition metals, lanthanide-ligand bonding has traditionally been viewed as predominantly ionic.[1, 2] However, recent work has shown that the 5d orbitals can play an important role in Ln-L bonding.[3-9] In addition, several studies have also identified the involvement of the 4f orbitals in Ce(IV)-L bonding.[3, 10-15] While our understanding of Ln-L bonding has increased substantially in recent years, experimental studies of covalency trends within the lanthanide series are still relatively rare.[16-21] In one example, Kozimor and co-workers used Cl K-edge XAS to evaluate Ln-Cl bonding within a series of $[LnCl_6]^{3-}$ complexes (Ln = Ce, Nd, Sm, Eu, Gd). They discovered modest mixing of the Cl 3p and Ln 5d orbitals, which decreased slightly on moving from Ce to Gd.[3] Calculations on the LnF_3 (Ln = La to Lu) series reveal a similar picture, namely that covalency in the Ln-F bonds is modest, primarily involves 2p/5d overlap, and is relatively constant across the series.[17] Additionally, the metal 4f contributions in the Ln-F covalency were shown to be sensitive to the Kohn-Sham delocalization error in density functional theory (DFT) calculations.[16]

NMR spectroscopy has recently emerged as a valuable method to gauge M-L covalency in the f elements, via the so-called SO-HALA effect (the spin-orbit (SO) coupling-induced heavy-atom (HA) effect on the light atom (LA) NMR chemical shift),[22-30] which causes the NMR resonance of a light atom bound to a heavy atom to shift to lower frequency ('downfield', i.e., a less shielded LA nucleus). The magnitude of this change in the chemical shift (Δ_{SO}) is dependent upon a number of factors, including the degree of HA-LA covalency.[31] This technique has been most commonly used to probe covalency in diamagnetic complexes with metal-carbon and metal-nitrogen bonds, due to the wide availability of the ^{13}C and ^{15}N isotopes,[32-46] but it has also been applied to other isotopes, including ^{1}H, ^{11}B, ^{19}F, ^{31}P, ^{29}Si, ^{77}Se, and ^{125}Te,[23, 47-53] demonstrating the versatility of this approach.

Previously, our group and others have shown that ^{13}C NMR spectroscopy could be used to analyze the covalency of the M-C bonds of organometallic lanthanide complexes.[15, 36, 45, 46, 54, 55] For example, a combined ^{13}C NMR spectroscopic and DFT computational analysis of $[Li(THF)_4][Ce^{IV}(\kappa^2\text{-}ortho\text{-oxa})(MBP)_2]$ (*ortho*-oxa = dihydro-dimethyl-2-[4-(trifluoromethyl)phenyl]-oxazolide and MBP^{2-} = 2,2′-methylenebis(6-*tert*-butyl-4-methylphenolate)), revealed a Δ_{SO} of 40 ppm for its C_{ipso} resonance, due to involvement of both 5d and 4f orbitals in the Ce-C bond.[46] Similarly, we used ^{13}C NMR spectroscopy and DFT to analyze the Ln-C bonds in $[Li(THF)_4][Ln(C_6Cl_5)_4]$ (Ln = La, Ce). This analysis revealed a Δ_{SO} of 9 ppm for the C_{ipso} resonance of the La analogue, which was due to a small amount of 5d covalency.[36] The ^{13}C NMR spectra of $[Ce^{IV}(CH_2{}^tBu)(NP{}^tBu_3)_3]$ and $[Ce^{IV}(BIPM^{TMS})_2]$ ($BIPM^{TMS}$ = $[C(PPh_2NSiMe_3)_2]^{2-}$) are also indicative of Ce-C covalency.[14, 45]

Herein, we report the synthesis and characterization of a series of Ln(III) Fmes complexes (FmesH = 1,3,5-$(CF_3)_3C_6H_3$). We chose to focus primarily on the lightest (La) and heaviest (Lu) lanthanides, in part because the diamagnetism of their +III oxidation state permits a detailed ^{13}C

NMR spectroscopic analysis, but also because the bonding differences between these two lanthanide ions should be maximized, potentially exposing unidentified trends in Ln covalency. Additionally, to our knowledge, a covalency analysis of Lu(III) using NMR spectroscopy has never been reported.

Results and Discussion

Synthesis. The reaction of $[LaI_3(THF)_4]$[56] with 4 equiv of LiFmes, generated *in situ*, in cold Et_2O (−25 °C) resulted in the immediate formation of a yellow solution concomitant with the deposition of a white precipitate. Work-up of this reaction after 10 min resulted in the isolation of $[Li(THF)_2(Et_2O)_2][La(Fmes)_4]$ ([Li][**1**]) as colorless blocks in 11% yield (Scheme 1). Similarly, reaction of $[Ce(NO_3)_3(THF)_4]$ with 4 equiv of LiFmes, generated *in situ*, in cold Et_2O/THF (−25 °C, 1:1 v/v) mixture resulted in an immediate color change to orange. Work-up of the reaction mixture after 5 min afforded $[Li(THF)_{3.5}(Et_2O)_{0.5}][Ce(Fmes)_4]$ ([Li][**2**]), which was isolated as a colorless mixture with unreacted LiFmes in low yield (Scheme 1). An ^{19}F NMR spectroscopic analysis of this mixture revealed the presence of [Li][**2**] and LiFmes in an approximate 1:1 ratio. Because of their similar solubilities, LiFmes always co-deposited alongside [Li][**2**], and due to their similar colors, their solids could not be physically separated. Thus, this material was characterized as a mixture (see below).

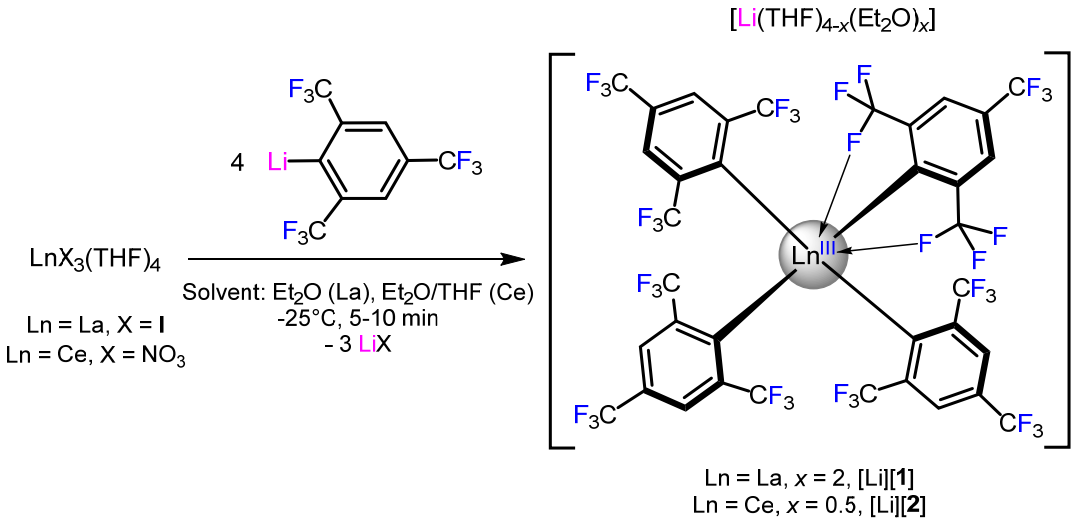

Scheme 1. Synthesis of [Li][**1**] and [Li][**2**]. Only two of eight F→Ln dative interactions are shown for clarity.

Additionally, we sought to extend this chemistry to lutetium. Thus, the reaction of $[Lu(NO_3)_3(THF)_3]$ with 4 equiv of *in situ* generated LiFmes, in cold Et_2O (−25 °C), resulted in the formation of $[Li(THF)_3][LuF(Fmes)_3]$ ([Li][**3**]), and not the expected complex, $[Lu(Fmes)_4]^-$. [Li][**3**] was also isolated as a colorless mixture with unreacted LiFmes in low yield (Scheme 2). A ^{19}F NMR spectrum of the isolated material revealed the presence of [Li][**3**] and LiFmes in an approximate 2:1 ratio. [Li][**3**] and LiFmes also displayed similar solubilities, necessitating their

characterization as a mixture. We also sought to isolate a lutetium perchlorophenyl complex, for comparison to the previously reported homoleptic Ln(III) aryl complexes, $[Li(THF)_4][Ln(C_6Cl_5)_4]$ (Ln = La, Ce).[36] Thus, reaction of $[Lu(NO_3)_3(THF)_3]$ with 4 equiv of *in situ* generated LiC_6Cl_5 and 3 equiv of DME, in cold Et_2O (−25 °C), resulted in formation of $[Li(DME)_3][Lu(C_6Cl_5)_4]$ ([Li][**4**]), which was isolated as colorless blocks in a 32% yield after work-up (Scheme 2). Note that low isolated yields were also observed for $[Li(THF)_4][Ln(C_6Cl_5)_4]$.[36]

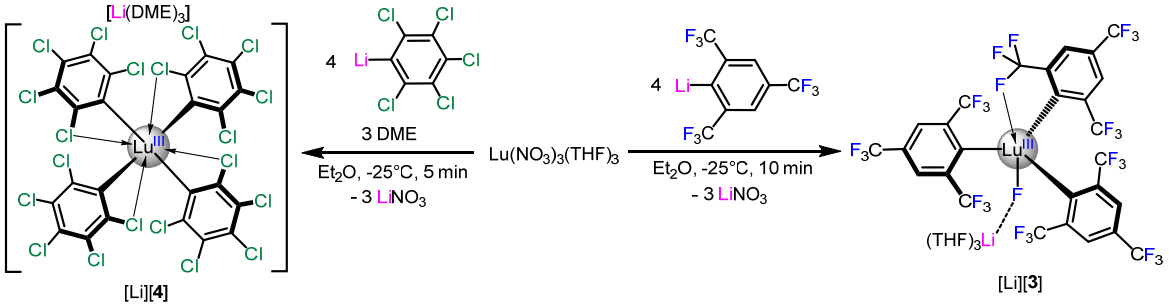

Scheme 2. Synthesis of [Li][**3**] and [Li][**4**]. For [Li][**3**], only one of three F→Ln dative interactions is shown for clarity.

The low yields for these complexes can be partially explained by their high thermal sensitivity, as they all display appreciable amounts of decomposition when monitored by NMR spectroscopy over time. For example, isolated samples of [Li][**1**], [Li][**2**], [Li][**3**] were dissolved in Et_2O-h_{10}/benzene-d_6 (9:1 v/v) at room temperature and monitored by ^{19}F NMR spectroscopy. The peaks assignable to each complex disappeared after ca. 6, 16, and 40 h, respectively (Figures S27, S29, S31, S32). Similarly, when an *in situ* generated sample of [Li][**4**] in Et_2O-h_{10}/benzene-d_6 (9:1 v/v) was monitored via $^{13}C\{^1H\}$ NMR spectroscopy, the peaks corresponding to [Li][**4**] completely disappeared after 42 h (Figure S35). In the case of [Li][**1**] and [Li][**2**], the only identifiable decomposition products are LiFmes and FmesH. In the case of [Li][**3**], we observe the formation of an unidentified Lu complex on standing for 1 h, as evidenced by the appearance of resonances at -20.9, -59.2, and -63.6 ppm in the ^{19}F NMR spectrum (Figures S31, S32). However, this complex completely decomposes after standing for 40 h at room temperature, forming LiFmes and FmesH as the only identifiable products. In the case of [Li][**4**], the only identifiable decomposition product is C_6Cl_5H.

The low yields of [Li][**1**]-[Li][**4**] are also partly due to the short reaction times, coupled with the low solubilities of the lanthanide salts in Et_2O. This combination of factors also explains the presence of unreacted LiFmes in isolated samples of [Li][**2**] and [Li][**3**]. However, longer reaction times resulted in complete decomposition of the targeted lanthanide organometallics. Decreasing the amount of LiFmes used in the reactions also resulted in lower yields. In the case of [Li][**1**], the use of $[LaI_3(THF)_4]$, which has marginally higher solubility than $[La(NO_3)_3(THF)_3]$ in Et_2O, was necessary to get any isolable product. In the case of [Li][**2**], the solubility of $[Ce(NO_3)_3(THF)_4]$ could be improved by addition of a small amount of THF to the

reaction mixture. However, this intervention did not work in the case of [Li][**1**] because of that complex's higher reactivity with THF (see below). The use of $CeCl_3$ as a starting material also failed, likely on account of its low solubility in Et_2O and Et_2O/THF mixtures.

Isolated, crystalline samples of [Li][**1**], [Li][**2**], and [Li][**3**] are insoluble in pentane, hexanes, toluene, and benzene, but highly soluble in Et_2O. Like its lanthanum and cerium analogs,[36] isolated samples of [Li][**4**] are insoluble in pentane, hexanes, toluene, and benzene, and Et_2O. In addition, complex [Li][**4**] rapidly decomposes upon dissolution in THF, as evidenced by the deposition of a black solid, necessitating its characterization *in situ* (see below). Complexes [Li][**1**], [Li][**2**], and [Li][**3**] also react with THF. For example, addition of excess THF to Et_2O-h_{10}/benzene-d_6 (9:1 v/v) solutions of [Li][**1**], [Li][**2**], and [Li][**3**] result in their complete disappearance after ca. 2.5, 7, and 18 h, respectively, according to ^{19}F NMR spectroscopy (Figures S28, S30, S33, S34). In the case of the reaction of [Li][**3**] with THF, we also observe formation of the same unidentified intermediate that was observed in the thermal decomposition.

X-ray Crystallography. Complexes [Li][**1**] and [Li][**2**] crystallize in the orthorhombic space group *Pbcn* (Figure 1). Their metal centers are coordinated by four *ipso*-carbon atoms of the Fmes ligands and eight F atoms of the *ortho*-CF_3 groups via long Ln─F contacts. According to the continuous shape measure,[57] [Li][**1**] and [Li][**2**] are best described as distorted O_h-symmetric cuboctahedrons (CSM: La = 0.99; Ce: 1.14). The average La–C distance in [Li][**1**] is 2.69 Å (Table 1), which is slightly longer than those seen in $[Li(THF)_4][La(C_6Cl_5)_4]$ (av. 2.594(3) Å)[36] and other σ-bonded lanthanum–aryl complexes, such as [{(*S,S*)-Phebox-^{i}Pr}$_3$La] ((S,S)-Phebox = (*S,S*)-2,6-bis(4′-isopropyl-2′-oxazolinyl)phenyl) (2.68 Å) and $[Cp_2La(2,6\text{-}(Me_2NCH_2)_2C_6H_3)]$ (2.548(3) Å), likely due to the greater steric bulk of Fmes.[58-60] The average Ce-C distance in [Li][**2**] (2.673 Å, Table 1) is also longer than those in $[Li(THF)_4][Ce(C_6Cl_5)_4]$ (av. 2.559(7) Å)[36] and other known σ-bonded cerium–aryl complexes such as Cp'$_2$Ce(C_6F_5) (Cp' = 1,3,4-^{t}Bu$_3$C$_5$H$_2$) (2.621(3) Å) and [Cp'$_2$Ce(2,3,4,6-C_6HF_4)] (2.623(3) Å).[61-63] The average F→La distance in [Li][**1**] is 2.868 Å, which is comparable to F→Ce distances in both [Li][**2**] (2.858 Å) and [Cp'$_2$Ce(2,3,4,5-C_6HF_4)] (2.87 Å).[63]

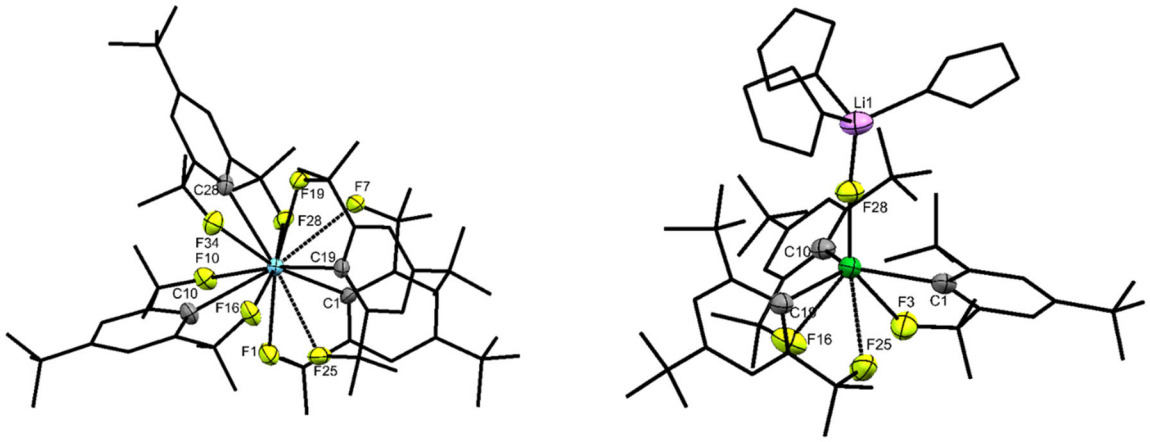

Figure 1. (left) Solid-state molecular structure of [Li][**1**] shown with 50% probability ellipsoids. Hydrogen atoms and $[Li(THF)_2(Et_2O)_2]^+$ counterion are omitted for clarity. Fmes ligands shown in wireframe. Only a single orientation of disordered CF_3 group is shown. (right) Solid-state molecular structure of [Li][**3**] shown with 50% probability ellipsoids. Hydrogen atoms are omitted for clarity, and the Fmes and THF ligands are shown in wireframe. Only a single orientation of the disordered CF_3 groups is shown.

Table 1. Selected bond lengths (Å) for [Li][**1**], [Li][**2**], and [Li][**3**].

Complex	[Li][**1**]	[Li][**2**]	[Li][**3**]
Ln-C	2.667(5), 2.704(5), 2.698(5), 2.689(6)	2.684(6), 2.677(7), 2.689(6), 2.640(6)	2.456(5), 2.445(5), 2.443(5)
F→Ln	2.839(3), 2.852(3), 2.946(3), 2.856(3), 2.882(3), 2.845(3), 2.824(3), 2.901(3)	2.884(4), 2.865(4), 2.891(4), 2.873(4), 2.828(4), 2.849(4), 2.824(4), 2.853(4)	2.594(3), 2.671(3), 2.641(3)
Lu-F	-	-	2.014(3)
Li-F	-	-	1.807(9)

Complex [Li][**3**] crystallizes in the monoclinic space group C2/c (Figure 1). The 7-coordinate metal center is bound by three *ipso*-carbons, three Lu─F dative interactions with the *ortho*-CF_3 groups, and one fluoride ligand, in a distorted capped octahedron geometry (CSM: 1.62).[57] It represents a rare example of a structurally-characterized lutetium fluoride coordination complex.[64, 65] The average Lu-C and F→Lu distances in [Li][**3**] are 2.45 Å and 2.64 Å (Table 1), respectively. The average Lu-C distance is comparable to those reported for other Lu-aryl complexes, such as $[Li(THF)_4][Lu(2,6\text{-}Me_2C_6H_3)_4]$ (av. 2.452 Å) and $Lu[o\text{-}C_6H_4CH_2NMe_2]_3$ (av. 2.435 Å).[66-68] The Lu1-F28 distance is 2.014(3) Å. This value is significantly shorter than the Lu-F distances in $[(NN^{TBS})Lu(\mu\text{-}F)(THF)]_2$ (H_2NN^{TBS} = fc(NHSi^{t}BuMe$_2$)$_2$) (av. 2.182(6) Å) and $[Lu_2(trans\text{-}1,2\text{-diaminocyclohexane})_2(\mu_2\text{-}F)_2(NO_3)_2][NO_3]_2$ (av. 2.20 Å).[64, 65] which both feature fluoride ligands bridged between Lu centers. Complex [Li][**3**] also features a close contact

between the $[Li(THF)_3]^+$ cation and fluoride ligand (Li1–F28 = 1.807(9) Å). This distance is within the range of known F→Li dative interactions.[69, 70]

The terminal fluoride ligand in [Li][**3**] is apparently derived from the Fmes fragment and represents a rare example of C-F bond activation by Lu^{3+}. We hypothesize that fluoride abstraction is driven by the fluorophilicity of the f elements,[71-74] coupled with the small ionic radius of Lu^{3+},[75] which cannot readily accommodate four bulky Fmes ligands, unlike La^{3+} and Ce^{3+}. This hypothesis is supported by the % buried volume of the Fmes ligand in [Li][**3**] (30.4%),[76] which is above the 25% threshold expected for formation of a stable homoleptic tetrakis complex (Figure S1). For comparison, the % buried volume of the $[C_6Cl_5]^-$ ligand in [Li][**4**] was calculated to be 25.6%,[76] rationalizing the ability for a single Lu^{3+} ion to coordinate four $[C_6Cl_5]^-$ ligands (Figure S1). The identity of the organic by-product of fluoride abstraction is currently unknown; however, its presence in the reaction mixture is evidenced by four unassigned peaks in the ^{19}F NMR spectrum of the crude reaction mixture, at -65.71, -65,78, -67.21, and -67.66 ppm. These peaks are present in an approximately 1:1:3:3 ratio, respectively (Figure S26).

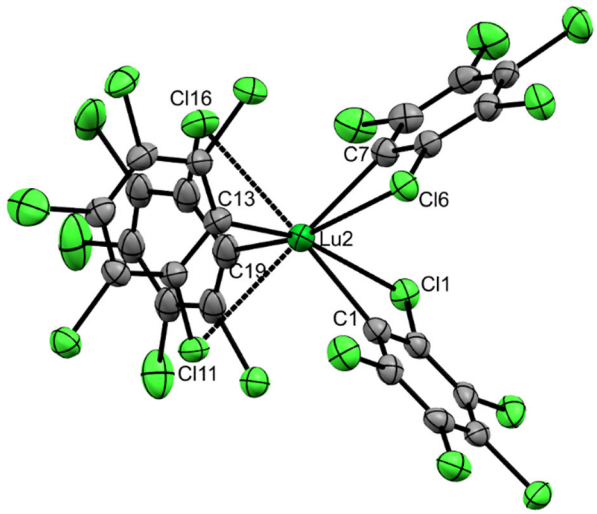

Figure 2. Solid-state molecular structure of [Li][**4**] shown with 50% probability ellipsoids. The $[Li(DME)_3]^+$ counterion was omitted for clarity. Selected bond lengths (Å) for [Li][**4**]: Lu2-C1 = 2.401(8), Lu2-C7 = 2.395(7), Lu2-C13 = 2.388(8), Lu2-C19 = 2.393(8), Lu2-Cl1 = 3.216(2), Lu2-Cl6 = 3.204(2), Lu2-Cl11 = 3.233(2), Lu2-Cl16 = 3.216(2).

Complex [Li][**4**] crystallizes in the monoclinic space group *C2/c* (Figure 2). The eight-coordinate metal center is bound by four *ipso*-carbons and four Cl→Lu dative interactions with the *ortho*-Cl atoms in a distorted T_d-symmetric triakis tetrahedral geometry, according to the continuous shape measure (CSM: 2.64).[57] The average Lu-C distance (2.39 Å) is slightly shorter than the average Lu-C distance found in [Li][**3**], but still within the range of known Lu-C_{aryl} distances.[66-68] The average Cl→Lu distance (3.217 Å) is significantly shorter than the those

observed in the isostructural La^{3+} (av. 3.52 Å) and Ce^{3+} (av. 3.51 Å) complexes,[36] likely due to the smaller ionic radius of Lu^{3+}.

NMR Characterization. NMR spectra for [Li][**1**], [Li][**2**], and [Li][**3**] were all collected at -35 °C, to minimize thermal decomposition, using isolated samples (as opposed to *in situ* generated material). Additionally, the spectra were recorded in Et_2O-h_{10}/benzene-d_6 (9:1 v/v) due to their poor solubility in arene solvents. The ^{1}H NMR spectrum of [Li][**1**] features a single resonance at 7.66 ppm, which is assignable to the *meta*-CH environment of the Fmes ligand (Figure S2). The *ortho*-CF_3 and *para*-CF_3 groups appear at -58.75 and -62.97 ppm, in a 2:1 ratio, in the ^{19}F NMR spectrum (Figure S3). A single resonance appears in the ^{7}Li{^{1}H} NMR spectrum at 0.35 ppm attributable to the Li^+ counterion (Figure S4). The *ipso*-carbon of the Fmes ligands appear as a triplet at 196.03 ppm in the ^{13}C{^{19}F} NMR spectrum (J_{CH} = 2.8 Hz) and as a broad singlet at 196.01 ppm in the ^{13}C{^{1}H} NMR spectrum (Figures S5, S7). For comparison, the *ipso*-carbon resonance of [Li(Et_2O)$_3$(THF)][UO_2(Fmes)$_3$] is shifted downfield substantially (240.03 ppm),[38] indicating a significant decrease in M-C covalency for [Li][**1**] (see below for further discussion).

The ^{1}H NMR spectrum of [Li][**2**] features a broad singlet at 13.69 ppm, which is assignable to the *meta*-CH resonance of the Fmes ligand (Figure S9). Its downfield shift can be attributed to the paramagnetism of the Ce^{3+} center. Also present in the spectrum are signals attributable to unreacted LiFmes and FmesH. The former could not be separated from [Li][**2**] due to its similar solubility, while the presence of the latter is likely due to thermal decomposition. Integration of their *meta*-CH resonances show that [Li][**2**], LiFmes, and FmesH are present in the 1:1:0.1 ratio, respectively. The ^{19}F NMR spectrum features broadened resonances at -60.95 and -79.92 ppm, in a 1:2 ratio, which are assignable to the *para*-CF_3 and *ortho*-CF_3 environments of the Fmes ligand, respectively (Figure S11). The ^{7}Li{^{1}H} NMR spectrum features a broad resonance at -3.31 ppm, attributable to the Li^+ counterion (Figure S12). The upfield shift and broadness of this signal may indicate the presence of a contact ion pair in solution.

The ^{1}H NMR spectrum of [Li][**3**] exhibits a resonance at 7.83 ppm, which is assignable to the *meta*-CH environment of the Fmes ligand (Figure S13). Similar to [Li][**2**], we also observed a signal attributable to unreacted LiFmes in the ^{1}H NMR spectrum. Integration of these resonances show that **3** and LiFmes are present in a 2:1 ratio, respectively. The ^{19}F{^{7}Li} NMR spectrum features a broad singlet at -32.26 ppm, a doublet at -59.41 ppm, and a singlet at -63.41 ppm (Figure S16). These resonances are present in a 1:18:9 ratio, and are assignable to the terminal fluoride, *ortho*-CF_3, and *para*-CF_3 environments, respectively. The peak ascribed to the terminal fluoride appears as a 1:1:1:1 quartet in the ^{19}F NMR spectrum ($J_{7\text{-LiF}}$ = 90.3 Hz), demonstrating that the contact ion pair present in the solid-state is maintained in solution (Figure S17). Our assignment is further buttressed by the observation of a doublet at -1.03 ppm ($J_{7\text{-LiF}}$ = 90.1 Hz) in the ^{7}Li{^{1}H} NMR spectrum (Figure S14). The doublet assignable to the *ortho*-CF_3 group (J_{FF} = 6.7 Hz), reveals coupling to the terminal fluoride ligand. Finally, the ^{13}C{^{19}F} and ^{13}C{^{1}H} NMR spectra of [Li][**3**] feature resonances at 191.84 and 191.82 ppm, respectively, which correspond to the *ipso*-carbon environment of the Fmes ligands (Figure S18, S20).

The $^{13}C\{^{1}H\}$ NMR spectrum of [Li][**4**], generated *in situ* (See SI for experimental details), was recorded in Et_2O-h_{10}/benzene-d_6 at -35 °C. It features a resonance at 185.34 ppm assignable to the *ipso*-carbon environment (Figure S24). This value is similar to the shift previously observed for the lanthanum analog (185.41 ppm), suggesting a similar degree of covalency.[36] The spectrum also displays peaks at 139.67, 130.80, and 130.15 ppm which we can ascribe to *ortho*-, *meta*-, and *para*-resonances of the pentachlorophenyl ligand, respectively. Additionally, we observed resonances assignable to unreacted LiC_6Cl_5.[36] The $^{7}Li\{^{1}H\}$ NMR spectrum features a single resonance at 0.07 ppm, attributable to the Li^+ counterion (Figure S22).

Computational Analysis. To understand the electronic structure and bonding interactions in [Li][**1**]-[Li][**4**], all-electron relativistic DFT calculations were performed on the anionic components of [Li][**1**], [Li][**2**], and [Li][**4**], and on the full contact ion pair structure of [Li][**3**], using various hybrid and non-hybrid functionals.[77] Complete computational details are provided in the Supporting Information. The following discussion focuses on the results obtained with the PBE functional.[78] A natural localized molecular orbital (NLMO)[79] analysis of the four La-C σ-bonds in [**1**]$^-$ reveals a density weight of ca. 9% of each of the relevant NLMOs at the La center (Figure 3). This weight corresponds to the share of electron density of these orbitals that is donated to La. Of the La weight, the 6s, 5d, and 4f shells contribute 13%, 75%, and 12%, respectively. The NLMO analysis furthermore identifies eight La-F orbital interactions, but with very weak covalency corresponding to only 1% La weight of each of the relevant fluorine lone-pair NLMOs. The NLMO analysis of the Ce-C σ-bonds in [**2**]$^-$ reveals comparable covalency as seen for [**1**]$^-$, with 10% Ce weight for each (Figure 3). The NLMO description of the eight Ce-F dative interactions also show minimal covalency, with only 1% Ce density weight for each (Figure S40).

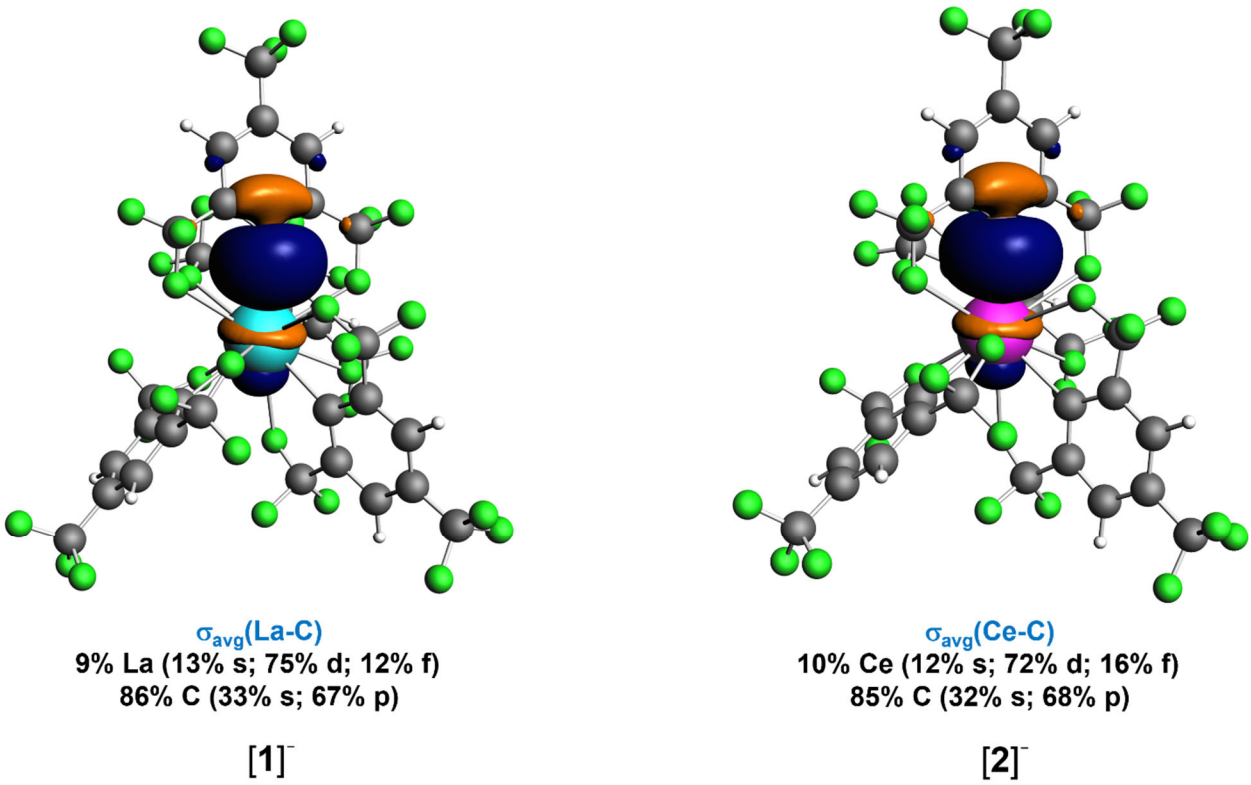

Figure 3. Representative Ln-L bonding NLMOs of [**1**]$^-$ and [**2**]$^-$ (isosurface values ±0.03 au). Orbital density weight % at the metal and carbon are listed along with atomic shell contributions (%) averaged over equivalent NLMOs. For [**2**]$^-$, values are additionally averaged over alpha and beta spin. Color code: La, sky blue; Ce, magenta; F, green; C, gray; H, white.

The NLMO analyses of the Lu-C σ-bonds in [Li][**3**] and [**4**]$^-$ reveal similar orbital compositions, with both having 9% Lu weights (Figure 4). The Lu-F covalency in [Li][**3**] has weaker electron density sharing with the metal in comparison, with 4% Lu weight of the σ-bonding NLMO (Figure 5). Consistent with past studies, the Lu-L bonding is dominated by the 5d orbitals; the 4f shell does not participate because of the radial contraction of 4f in the late lanthanides[80, 81] and the fact that the Lu(III) 4f shell is completely filled. There are also two equivalent fluorine lone-pair NLMOs that show weak π-bonding, as evidenced by their 2% Lu weights. The NLMO analysis additionally reveals weak Cl→Lu dative interactions in [**4**]$^-$, with average Lu density weights of 2% of the corresponding Cl-centered lone-pair NLMOs (Figure S41) The density sharing with the metal by the Cl substituents is therefore somewhat stronger than what was found for CF_3 in [Li][**3**]. This finding is supported by the second-order perturbation theory analysis of the donor-acceptor delocalization energies from the NBO calculation: the strongest Cl(donor)→Lu(acceptor) dative interaction in [**4**]$^-$ is calculated to be 7.7 kcal/mol, which is 2.1 kcal/mol greater than that of the strongest CF_3(donor)→Lu(acceptor) interaction in [Li][**3**]. Additionally, the 2% average Lu weight of the Cl→Lu dative interactions is similar to the metal weights previously found for the isostructural La and Ce analogues.[36]

Overall, for the four complexes, the % metal weights of the M-C σ-bond orbitals, indicating the fractions of density that are covalently shared with the metal, are similar (9-10%). Additionally, [**1**]$^-$ and [**2**]$^-$ feature notable 4f-shell participation in those bonds, whereas for the $4f^{14}$ complexes, [Li][**3**] and [**4**]$^-$, the calculations do not indicate 4f participation in the metal-ligand bonds, as expected. Furthermore, the calculations show that the Lu-F bonding NLMOs in [Li][**3**] are considerably more strongly polarized toward the ligand than the Ln-C bonds, in line with the high electronegativity of fluorine.

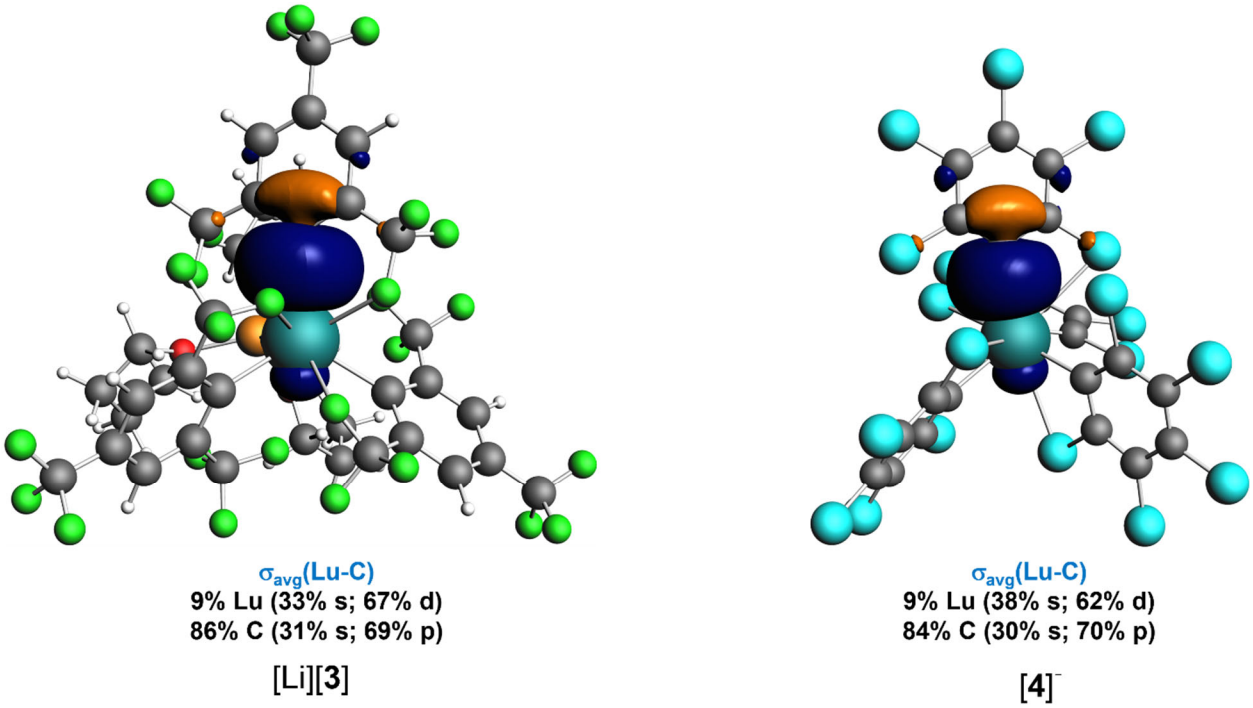

Figure 4. Representative Lu–C bonding NLMOs of [Li][**3**] and [**4**]$^-$ (isosurface values ±0.03 au). Orbital density weight % at the metal and carbon are listed along with atomic valence shell contributions (%) averaged over equivalent NLMOs. Color code: Lu, dark cyan; F, green; C, gray; H, white.

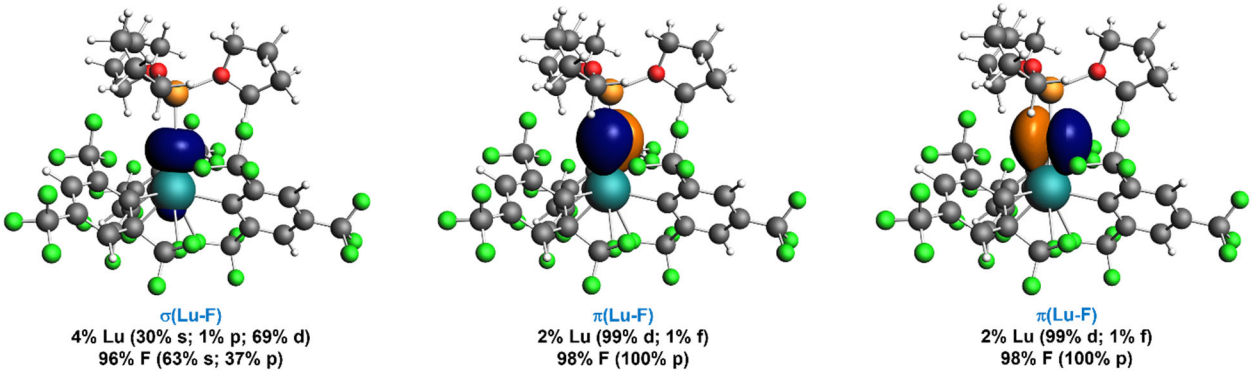

Figure 5. Representative Lu–F-interacting NLMOs in [Li][**3**] (isosurface values ±0.03 au.). Orbital density weight % at the metal and fluorine are listed along with atomic valence shell contributions (%). Color code: Lu, dark cyan; F, green; C, gray; H, white.

We also calculated the ^{13}C NMR chemical shifts of the C_{ipso} sites for [**1**]$^-$, [Li][**3**], and [**4**]$^-$, with and without SO effects. No ^{13}C NMR spectrum could be obtained for [Li][**2**] because of its paramagnetism. Accordingly, chemical shifts for [**2**]$^-$ were not calculated. Since the experimental NMR measurements were performed in a benzene/Et_2O mixture, two sets of calculated NMR data are provided (Tables S3 and S4), using continuum solvent models for benzene and Et_2O, respectively. The calculated chemical shifts with the two solvent models are very similar, and therefore only the results for benzene are discussed herein. The calculated C_{ipso} chemical shift for [**1**]$^-$ is 210 ppm (expt. = 196.03 ppm), which includes a 9.6 ppm deshielding due to SO effects. The calculated C_{ipso} chemical shift for [Li][**3**] is 198.7 ppm and in better agreement with experiment (191.84 ppm). This value includes a 13.4 ppm deshielding attributable SO effects. The calculated C_{ipso} chemical shift for [**4**]$^-$ is 187.1 (exp = 185.34 ppm), which includes a 12.1 ppm deshielding due to SO effects. Attempts to improve the calculated chemical shifts for the Fmes complexes toward the experimental data by using different approximate functionals or intermediate (secondary) NMR references were unsuccessful. The deviations between the calculated and experimental NMR shifts may potentially be due to dynamics, which was not modeled explicitly. Another possibility is that the large number of fluorine substituents on Fmes affect the description of the dynamic correlation by the approximate functionals. Nonetheless, the calculations give useful insight, namely, that the calculated SO effects on the C_{ipso} NMR chemical shifts across these three complexes are similar (10-14 ppm), and also of comparable magnitude, if somewhat larger, to the Δ_{SO} value calculated for lanthanum analogue of [**4**]$^-$, $[La(C_6Cl_5)_4]^-$ (8 ppm).[36] The similarity of the SO shielding effects is broadly consistent with the comparable metal-carbon covalency found in the calculations. However, if one assumes that these effects predominantly arise from f-orbital involvement in bonding, the similar magnitude of SO effects on the C_{ipso} NMR shifts for the La and Lu complexes is surprising, because the 4f-shell contributions to the Ln- C_{ipso} bonds in [Li][**3**] and [**4**]$^-$ are negligible. However, it is important to note that the 5d orbitals can also contribute to the SO effect, and since Lu (Z = 71) has a higher atomic number than La (Z = 57), and therefore stronger relativistic effects overall,

its higher Z further strengthens the SO contribution to the chemical shifts. The relative strengths of SO effects on ligand NMR shifts induced by the valence f vs. d shells of a covalently bound metal center will be investigated in more detail in an upcoming publication.

We also calculated the ^{19}F NMR chemical shift of the terminal fluoride in [Li][**3**], providing a unique opportunity to gauge M-L covalency in the same complex using two different nuclei. The calculated ^{19}F chemical shift is -29.4 ppm, which is in reasonably good agreement with the experimental shift (-32.26 ppm). The calculated shift includes 5.5 ppm deshielding attributable to SO effects. The relatively small SO contribution to this shift can be rationalized by the weaker covalent character of the Lu-F bond in this complex, as compared to Lu-C.

Conclusion

We have prepared a series of novel Ln aryl complexes, namely, $[Ln(Fmes)_4]^-$ (Ln = La, Ce), $[LuF(Fmes)_3]^-$, and $[Lu(C_6Cl_5)_4]^-$, and evaluated the covalency of their Ln-C_{ipso} and Lu-F bonds using a combination of multi-nuclear NMR spectroscopy and relativistic DFT calculations. This analysis revealed a comparable degree of overall Ln-C_{ipso} covalency for La, Ce, and Lu, as quantified by the metal center's share of electron density in the orbitals that describe the Ln-C_{ipso} bonds. The calculations also indicate that the Ln component is predominately 5d in character; however, the La-C_{ipso} and Ce-C_{ipso} bonds do exhibit a small amount of 4f orbital participation. In contrast, the Lu-C_{ipso} bonds have no 4f character, as expected. Despite this difference, the calculated spin-orbit deshielding effects on the C_{ipso} ^{13}C chemical shifts are similar between the La and Lu complexes, pointing to the important role that the 5d orbitals and atomic number (Z) play in NMR shielding.

Experimental Section

General. All reactions and subsequent manipulations were performed under anaerobic and anhydrous conditions under an atmosphere of dinitrogen. Hexanes, diethyl ether (Et_2O), and toluene were dried using a Vacuum Atmospheres DRI-SOLV Solvent Purification system and stored over 3Å sieves for 24 h prior to use. Tetrahydrofuran (THF) was distilled over Na/benzophenone and stored over activated 3 Å molecular sieves for 24 h prior to use. Benzene-*d*$_6$ was dried over 3Å molecular sieves for 24 h prior to use. LaI_3,[82] $[Ce(NO_3)_3(THF)_4]$,[83] and $[Lu(NO_3)_3(THF)_3]$[83] were synthesized according to the previously reported procedures. All other reagents were purchased from commercial suppliers and used as received.

^{1}H, ^{13}C{^{1}H}, ^{13}C{^{19}F}, ^{19}F{^{7}Li}, ^{19}F, and ^{7}Li{^{1}H} NMR spectra were recorded on a Bruker AVANCE NEO 400 MHz spectrometer or a Bruker AVANCE NEO 500 MHz spectrometer. ^{1}H, ^{13}C{^{1}H}, and ^{13}C{^{19}F} NMR spectra were referenced to external tetramethylsilane (TMS) using the residual protio solvent peaks as internal standards. ^{7}Li{^{1}H}, ^{7}Li{^{19}F}, ^{19}F{^{7}Li} and ^{19}F NMR spectra were referenced indirectly with the ^{1}H chemical shift of TMS at 0 ppm, according to IUPAC standard.[84, 85] IR spectra were recorded on a Nicolet Summit X FT-IR spectrometer. Elemental analyses were performed by the Microanalytical Laboratory at the University of California (Berkeley, CA).

Synthesis of LiFmes. The synthesis of LiFmes was performed according to the literature procedure with slight modifications.[86] *Caution! Trifluoromethylaryl lithium reagents can reportedly detonate upon isolation from ethereal solvents.*[87] *Accordingly, LiFmes was only handled in situ.* A cold solution (–25 °C) of *n*-BuLi in hexanes (0.2 mL, 0.50 mmol, 2.5 M) was added dropwise to a cold, stirring solution (–25 °C) of 1,3,5-$(CF_3)_3C_6H_3$ (0.093 mL, 0.50 mmol) in Et_2O (2 mL). After 30 min of stirring at 25 °C, the reaction mixture became a clear pale-yellow color. The resulting LiFmes solution was used as is, and assumed to be 0.25 M.

Synthesis of LiC_6Cl_5. The synthesis of LiC_6Cl_5 was performed according to the literature procedure with slight modifications.[88] *Caution! LiC_6Cl_5 reportedly detonates upon attempted isolation from ethereal solvents.*[89] *Accordingly, it was only handled in situ.* A cold solution (–25 °C) of *n*-BuLi in hexanes (0.2 mL, 0.50 mmol, 2.5 M) was added dropwise to a cold, stirring suspension (–25 °C) of C_6Cl_6 (142.4 mg, 0.50 mmol) in Et_2O (2 mL). Upon addition of *n*-BuLi, the solids dissolved and the solution became a golden color. The resulting LiC_6Cl_5 solution was used immediately, as prepared, and assumed to be 0.25 M.

Synthesis of $[LaI_3(THF)_4]$. The synthesis of $[LaI_3(THF)_4]$ was performed according to the literature procedure with slight modifications.[56] A sample of LaI_3 (570.3 mg, 1.1 mmol) was dissolved in THF (12 mL) and allowed to stir for 30 min. Immediately upon addition of THF, a white solid began precipitating from solution. The volatiles were then removed *in vacuo* to provide a white powder (490 mg, 55% yield). A small amount of white powder (10 mg) was dissolved in THF (1 mL) and cooled to –25 °C for 12 h, which resulted in the deposition of colorless crystals. The unit cell of a crystal was determined by X-ray crystallography (a = 8.775(3) Å, b = 17.672(3) Å, c = 16.729(4) Å, α = 90°, β = 90°, γ = 93.74°), which matched the reported cell.[90]

Synthesis of $[Li(THF)_2(Et_2O)_2][La(Fmes)_4]$ ([Li][1]). A cold (–25 °C) solution of LiFmes (2.3 mL in Et_2O, 0.575 mmol, 0.25 M) was added to a cold (–25 °C), stirring suspension of $[LaI_3(THF)_4]$ (115.1 mg, 0.142 mmol) in Et_2O (2 mL), which resulted in an immediate color change to pale yellow, concomitant with the deposition of a flocculent white precipitate. After 2 min of stirring, the volatiles were removed *in vacuo* to provide a pale-yellow solid, which was triturated with cold (–25 °C) pentane (2 × 1 mL). The solid was then extracted into pentane (2 mL) and filtered through a Celite column (0.5 cm × 5 cm) supported on glass wool to afford a clear yellow filtrate. The volume of the filtrate was reduced to 1 mL *in vacuo* and the sample was stored at –25 °C for 24 h, which resulted in the deposition of colorless blocks. The solid was isolated by decanting the supernatant, washing with pentane and then drying briefly *in vacuo* (24.5 mg, 11% yield). ^{1}H NMR (500 MHz, –35 °C, Et_2O-h_{10}/benzene-d_6): δ 7.66 (s, *m*-H). $^{13}C\{^{19}F\}$ NMR (125.8 MHz, –35 °C, Et_2O-h_{10}/benzene-d_6): δ 196.03 (t, J_{CH} = 2.8 Hz *i*-C), 139.24 (s, *o*-CF_3), 129.86 (s, *o*-C), 128.97 (s, *p*-CF_3), 124.44 (t, J_{CH} = 4.3 Hz, *p*-C), 123.33 (dd, J_{CH} = 5.7, 159.2 Hz *m*-C). $^{13}C\{^1H\}$ NMR (125.8 MHz, –35 °C, Et_2O-h_{10}/benzene-d_6): δ 196.01 (br s, *i*-C), 139.24 (br s, *o*-CF_3), 130.94 (s, *o*-C), 128.74 (q, J_{CF} = 34.0 Hz, *p*-CF_3), 125.52 (s, *p*-C), 123.36 (s, *m*-C). ^{19}F NMR (470.6 MHz, –35 °C, Et_2O-h_{10}/benzene-d_6): δ -58.75 (s, 24F, *o*-CF_3), -62.97 (s, 12F, *p*-CF_3). $^7Li\{^1H\}$ NMR (194.4 MHz, –35 °C, Et_2O-h_{10}/benzene-d_6): δ 0.35 (s). IR (KBr pellet, cm^{-1}): 2983 (m), 2884 (m), 1822 (vw), 1614 (m), 1556 (w), 1460 (w), 1386 (w), 1299 (s), 1276 (s), 1255 (s), 1183 (s), 1151 (s), 1121 (s), 1089 (m), 1040 (s), 907 (m), 889 (m), 842 (s), 731 (w), 684 (s), 552 (w), 498 (w).

Synthesis of [Li(THF)$_{3.5}$(Et$_2$O)$_{0.5}$][Ce(Fmes)$_4$] ([Li][2]). A cold (–25 °C) solution of LiFmes (2.5 mL in Et$_2$O, 0.64 mmol, 0.25 M) was added to a cold (–25 °C), stirring suspension of [Ce(NO$_3$)$_3$(THF)$_4$] (98.3 mg, 0.16 mmol) in Et$_2$O (1 mL) and THF (1 mL), which resulted in an immediate color change to orange, concomitant with the deposition of a fine white precipitate. After 3 min of stirring, the volatiles were removed *in vacuo* to provide a yellow tacky oil. The oil was extracted into cold Et$_2$O (–25 °C; 2 mL) and filtered through a Celite column (0.5 cm × 5 cm) supported on glass wool to afford a clear yellow filtrate. The volatiles were removed *in vacuo* and the resulting tacky oil was triturated with cold pentane (–25 °C; 2 × 1 mL) to yield a pale-yellow oil. The oil was then extracted into cold pentane (–25 °C; 3 mL), the volume of the filtrate was reduced to 1 mL *in vacuo*, and the sample was stored at –25 °C for 24 h, which resulted in the deposition of colorless blocks. The solid was isolated by decanting the supernatant, washing with cold pentane (1 mL), and then drying briefly *in vacuo* (Yield: 25 mg). A ^{1}H NMR analysis of this solid revealed the presence of [Li][**2**] and LiFmes in an approximate 1:1 molar ratio, which corresponds to an overall 8% yield of [Li][**2**]. ^{1}H NMR (500 MHz, –35 °C, Et$_2$O-h_{10}/benzene-d_6): δ 13.69 (br s, *m*-H, [Li][**2**]) 7.65 (s, *m*-H, LiFmes). ^{19}F NMR (470.6 MHz, –35 °C, Et$_2$O-h_{10}/benzene-d_6): δ -60.95 (s, 12F, *p*-CF$_3$, [Li][**2**]), -79.92 (br s, 24F, *o*-CF$_3$, [Li][**2**]) -63.05 (s, *o*-CF$_3$, LiFmes), -63.15 (s, *p*-CF$_3$, LiFmes). ^{7}Li{^{1}H} NMR (194.4 MHz, –35 °C Et$_2$O-h_{10}/benzene-d_6): δ -3.31 (br s, [Li][**2**]), 1.27 (s, LiFmes). IR (KBr pellet, cm^{-1}): 2964 (m), 2962 (m), 2890 (m), 2221 (vw), 2110 (vw), 1821 (w), 1614 (s), 1536 (m), 1464 (m), 1395 (m), 1291 (vs), 1273 (vs), 1199 (vs), 1192 (vs), 1140 (vs), 1091 (vs), 1042 (s), 1000 (m), 907 (s), 889 (m), 843 (s), 839 (s), 732 (m), 685 (vs), 666 (m), 554 (w), 503 (m), 424 (m).

Synthesis of [Li(THF)$_3$][LuF(Fmes)$_3$] ([Li][3]). A cold (–25 °C) solution of LiFmes (2.9 mL in Et$_2$O, 0.725 mmol, 0.25 M) was added to a cold (–25 °C), stirring suspension of [Lu(NO$_3$)$_3$(THF)$_3$] (104.6 mg, 0.181 mmol) in Et$_2$O (2 mL), which resulted in an immediate color change to pale yellow, concomitant with the deposition of a flocculent white precipitate. After 5 min of stirring, the reaction mixture was filtered through a Celite column (0.5 cm × 5 cm) supported on glass wool to afford a clear yellow filtrate. The volatiles were removed in vacuo and the resulting white powder was extracted into cold (–25 °C) pentane (3 mL) and filtered through a Celite column (0.5 cm × 5 cm) supported on glass wool to afford a clear yellow filtrate. The solution was concentrated to ~1 mL, and the resulting solution was stored at –25 °C for 24 h, which resulted in the deposition of colorless blocks. The solid was isolated by decanting the supernatant, washing the crystals with a cold (–25 °C) 1:1 Et$_2$O/pentane solution (1 mL), and drying briefly *in vacuo* (Yield: 71 mg). A ^{1}H NMR analysis revealed the presence of [Li][**3**] and LiFmes in an approximate 2:1 ratio, which corresponds to an overall 24% yield of [Li][**3**]. ^{1}H NMR (500 MHz, –35 °C, Et$_2$O-h_{10}/benzene-d_6): δ 7.83 (s, *m*-H, [Li][**3**]), 7.65 (s, *m*-H, LiFmes). ^{13}C{^{19}F} NMR (125.8 MHz, –35 °C, Et$_2$O-h_{10}/benzene-d_6): δ 191.84 (t, J_{CH} = 3.2 Hz, *i*-C, [Li][**3**]), 141.97 (s, *o*-CF$_3$, LiFmes), 139.48 (s, *o*-CF$_3$, [Li][**3**]), 129.45 (s, *p*-CF$_3$, [Li][**3**]), 128.57 (s, *o*-C, [Li][**3**]), 127.43 (s, *o*-C, LiFmes), 126.66 (s, *p*-CF$_3$, LiFmes), 125.12 (t, J_{CH} = 4.3 Hz, *p*-C, LiFmes) 124.11 (t, J_{CH} = 4.3 Hz, *p*-C, [Li][**3**]), 123.97 (dd, J_{CH} = 5.99, 162.1 Hz, *m*-C, [Li][**3**]), 120.48 (dd, J_{CH} = 4.8, 158.4, *m*-C, LiFmes). ^{13}C{^{1}H} NMR (125.8 MHz, –35 °C, Et$_2$O-h_{10}/benzene-d_6): δ 191.82 (*s*, *i*-C, [Li][**3**]), 142.08 (q, J_{CF} = 27.69 Hz, *o*-CF$_3$, LiFmes), 139.36 (q, J_{CF} = 29.89 Hz, *o*-CF$_3$, [Li][**3**]), 129.67 (s, *o*-C, [Li][**3**]), 129.59 (q, J_{CF} = 33.27 Hz, *p*-CF$_3$, [Li][**3**]), 127.50 (s, *o*-C, LiFmes), 126.80 (q, J_{CF} = 30.99 Hz, *p*-CF$_3$, LiFmes), 125.19 (m, *p*-C, LiFmes), 123.93 (s, *m*-C, [Li][**3**]), 123.03 (s, *p*-C, [Li][**3**]), 120.45 (s, *m*-C, LiFmes). ^{19}F{^{7}Li} NMR (470.56 MHz, –35 °C, Et$_2$O-h_{10}/benzene-d_6): δ -32.26 (br s, 1F, Lu-F, [Li][**3**]), -59.41 (d, J_{FF} = 6.72 Hz, 18F, *o*-CF$_3$, [Li][**3**]), -63.01 (s, *o*-CF$_3$, LiFmes), -63.12 (s, *p*-CF$_3$, LiFmes) -63.41 (s, 9F, *p*-CF$_3$, [Li][**3**]). ^{19}F NMR (470.56 MHz, –35 °C, Et$_2$O-h_{10}/benzene-

d_6): δ -32.35 (q, J_{LiF} = 90.3 Hz, 1F, Lu-F, [Li][**3**]), -59.41 (d, J_{FF} = 6.72 Hz, 18F, *o*-CF_3, [Li][**3**]), -63.01 (s, *o*-CF_3, LiFmes), -63.12 (s, *p*-CF_3, LiFmes) -63.41 (s, 9F, *p*-CF_3, [Li][**3**]). $^7Li\{^1H\}$ NMR (194.4 MHz, –35 °C, Et_2O-h_{10}/benzene-d_6): δ -1.03 (d, J_{LiF} = 90.1 Hz, [Li][**3**]), 1.27 (s, LiFmes). $^7Li\{^{19}F\}$ NMR (194.4 MHz, –35 °C, Et_2O-h_{10}/benzene-d_6): δ -0.90 (s, [Li][**3**]), 1.29 (s, LiFmes). IR (KBr pellet, cm^{-1}): 3082 (vw), 2962 (m) 2932 (m), 2875 (m), 1829 (w), 1641 (w), 1620 (m), 1588 (w), 1559 (m), 1461 (m), 1419 (m), 1395 (m), 1378 (m), 1300 (s), 1276 (s), 1257 (s), 1189 (s), 1119 (s), 1092 (s), 1042 (m), 1010 (w), 960 (vw), 909 (s), 889 (w), 845 (s), 834 (m), 732 (m), 686 (s), 667 (m), 553 (w), 505 (w), 426 (m).

Synthesis of [Li(DME)$_3$][Lu(C$_6$Cl$_5$)$_4$] ([Li][4]). A cold (–25 °C) solution of LiC_6Cl_5 (1.4 mL in Et_2O, 0.348 mmol, 0.25 M) was added to a cold (–25 °C), stirring suspension of $[Lu(NO_3)_3(THF)_3]$ (50.5 mg, 0.087 mmol) in Et_2O (2 mL) and DME (0.029 mL, 0.28 mmol), which resulted in an immediate color change to brown-orange, concomitant with the deposition of a flocculent brown precipitate. After 5 min of stirring, the reaction mixture was filtered through a Celite column (0.5 cm × 5 cm) supported on glass wool to afford a clear brown-orange filtrate. The volatiles were removed *in vacuo* and the resulting oil was extracted into cold toluene (–25 °C; 3 mL). The volume of the solution was reduced to 1 mL *in vacuo* and the sample was stored at –25 °C for 24 h, which resulted in the deposition of colorless plates. The solid was isolated by decanting the supernatant and then drying briefly *in vacuo* (40.3 mg, 32% yield). Anal. Calcd for $LuC_{36}H_{30}Cl_{20}LiO_6$: C, 29.83; H, 2.09. Found: C, 29.12; H, 2.04. IR (KBr pellet, cm^{-1}): 3110 (vw), 3065 (vw), 2965 (vw), 2925 (w), 2877 (vw), 2829 (vw), 2827 (vw), 2358 (vw), 2337 (vw), 1558 (w), 1506 (w), 1456 (w), 1397 (m), 1333 (m), 1309 (m), 1282 (s), 1227 (w), 1171 (m), 1123 (w), 1085 (s), 1057 (m), 1030 (w), 865 (m), 820 (s), 683 (m), 658 (m), 562 (w), 525 (vw), 465 (vw), 417 (vw).

***In Situ* Preparation of [Li(DME)$_3$][Lu(C$_6$Cl$_5$)$_4$] ([Li][4]).** A cold (–25 °C) solution of LiC_6Cl_5 (2.2 mL in Et_2O, 0.54 mmol, 0.25 M) was added to a cold (–25 °C), stirring suspension of $[Lu(NO_3)_3(THF)_3]$ (77.8 mg, 0.135 mmol) in Et_2O (2 mL) and DME (0.042 mL, 0.404 mmol). After 5 min, the reaction mixture was filtered through a Celite column (0.5 cm × 5 cm) supported on glass wool to afford an orange-brown filtrate. The volume of the filtrate was reduced to 1 mL in vacuo. An aliquot (0.6 mL) of the concentrated reaction filtrate and 4 drops (ca. 0.03 mL) of benzene-d_6 was then transferred to an NMR tube and NMR spectra were recorded. $^{13}C\{^1H\}$ NMR (125.8 MHz, –35 °C, Et_2O-h_{10}/benzene-d_6): δ 186.26 (s, *i*-C, LiC_6Cl_5), 185.34 (s, *i*-C, [Li][**4**]), 141.23 (s, *o*-C, LiC_6Cl_5), 139.67 (s, *o*-C, [Li][**4**]), 130.80 (s, *m*-C, [Li][**4**]), 130.15 (s, *p*-C, [Li][**4**]), 127.60 (s, *m*-C, LiC_6Cl_5), 126.89 (s, *p*-C, LiC_6Cl_5). $^7Li\{^1H\}$ NMR (194.4 MHz, –35 °C, Et_2O-h_{10}/benzene-d_6): δ 0.07 (s).

ASSOCIATED CONTENT

Supporting Information

Additional experimental procedures, crystallographic details, spectral data, and computational details for complexes [Li][**1**]–[Li][**4**] (PDF).

Author Information

Corresponding Authors

Jochen Autschbach - *Department of Chemistry, University at Buffalo, State University of New York, Buffalo, New York 14260, United States;*

Trevor W. Hayton - *Department of Chemistry and Biochemistry, University of California Santa Barbara, Santa Barbara, California 93106, United States*;

Authors

Grant Dickinson - *Department of Chemistry and Biochemistry, University of California Santa Barbara, Santa Barbara, California 93106, United States;*

Xiaojuan Yu - *Department of Chemistry, University at Buffalo, State University of New York, Buffalo, New York 14260, United States*;

Guang Wu - *Department of Chemistry and Biochemistry, University of California Santa Barbara, Santa Barbara, California 93106, United States*

Cary R. Stennett - *Department of Chemistry, University of California, Irvine, California 92697-2025, United States*;

Acknowledgement

This synthesis portion of this work was supported by the NSF-CHE 2350218. J.A. acknowledges financial support from the U.S. Department of Energy, Office of Basic Energy Sciences, Heavy Element Chemistry program, grant DE-SC0001136 for the theoretical component of this study. This research made use of the 400 MHz NMR spectrometer in the Department of Chemistry, an NIH SIG (1S10OD012077-01A1), and a 500 MHz NMR spectrometer supported by an NSF Major Research Instrumentation (MRI) Award 1920299. Support for C.R.S. and preparation of the LaI_3 used in this study was provided under NSF-CHE 2452677 (to W. J. Evans at UC Irvine).

References

1. Vitova, T.; Roesky, P. W.; Dehnen, S., Open questions on bonding involving lanthanide atoms. *Commun. Chem.* **2022**, *5*, 12.
2. Zhu, Q.; Zhu, J.; Zhu, C., Recent progress in the chemistry of lanthanide-ligand multiple bonds. *Tetrahedron Lett.* **2018**, *59*, 514-520.
3. Löble, M. W.; Keith, J. M.; Altman, A. B.; Stieber, S. C. E.; Batista, E. R.; Boland, K. S.; Conradson, S. D.; Clark, D. L.; Lezama Pacheco, J.; Kozimor, S. A.; Martin, R. L.; Minasian, S. G.; Olson, A. C.; Scott, B. L.; Shuh, D. K.; Tyliszczak, T.; Wilkerson, M. P.; Zehnder, R. A., Covalency in Lanthanides. An X-ray Absorption Spectroscopy and Density Functional Theory Study of $LnCl_6^{x-}$ (x = 3, 2). *J. Am. Chem. Soc.* **2015**, *137*, 2506-2523.
4. Mooßen, O.; Dolg, M., Two interpretations of the cerocene electronic ground state. *Chemical Physics Letters* **2014**, *594*, 47-50.
5. Kaltsoyannis, N.; Bursten, B. E., Electronic structure of f^1 lanthanide and actinide complexes. Part 2. Non-relativistic and relativistic calculations of the ground state electronic structures and optical transition energies of [Ce(η-C_5H_5)$_3$], [Th(η-C_5H_5)$_3$] and [Pa(η-C_8H_8)$_2$]. *J. Organomet. Chem.* **1997**, *528*, 19-33.
6. Hazin, P. N.; Bruno, J. W.; Brittain, H. G., Luminescence spectra of a series of cerium(III) halides and organometallics. Probes of bonding properties using 4f-5d excited states. *Organometallics* **1987**, *6*, 913-918.
7. Atanasov, M.; Daul, C.; Güdel, H. U.; Wesolowski, T. A.; Zbiri, M., Ground States, Excited States, and Metal−Ligand Bonding in Rare Earth Hexachloro Complexes: A DFT-Based Ligand Field Study. *Inorg. Chem.* **2005**, *44*, 2954-2963.
8. Kerridge, A., Oxidation state and covalency in f-element metallocenes (M = Ce, Th, Pu): a combined CASSCF and topological study. *Dalton Trans.* **2013**, *42*, 16428-16436.
9. Clark, D. L.; Gordon, J. C.; Hay, P. J.; Poli, R., Existence and Stability of Lanthanide−Main Group Element Multiple Bonds. New Paradigms in the Bonding of the 4f Elements. A DFT Study of Cp_2CeZ (Z = F^+, O, NH, CH^-, CH_2) and the Ligand Adduct $Cp_2Ce(CH_2)(NH_3)$. *Organometallics* **2005**, *24*, 5747-5758.
10. Branson, J. A.; Smith, P. W.; Sergentu, D.-C.; Russo, D. R.; Gupta, H.; Booth, C. H.; Arnold, J.; Schelter, E. J.; Autschbach, J.; Minasian, S. G., The Counterintuitive Relationship between Orbital Energy, Orbital Overlap, and Bond Covalency in CeF_6^{2-} and $CeCl_6^{2-}$. *J. Am. Chem. Soc.* **2024**, *146*, 25640-25655.
11. Smith, P. W.; Sergentu, D.-C.; Branson, J. A.; Russo, D. R.; Booth, C. H.; Autschbach, J.; Minasian, S. G., 4f-Orbital Occupancy in Tetravalent Cerium Halide Complexes from X-ray Spectroscopy and Theory. *Inorg. Chem.* **2025**, *64*, 18091-18102.
12. Pérez Bedwell, G.; Suryadevara, N.; Qi, Z.; Gable, R. W.; Bencok, P.; Baker, M. L.; Boskovic, C., Tuning the Electronic Properties of Tetravalent Cerium Complexes via Ligand Derivatization. *Inorg. Chem.* **2025**, *64*, 6519-6530.
13. Tateyama, H.; Liao, C.; Wilkinson, G. R.; Ramanathan, A.; Amidani, L.; Bazarkina, E.; Ressnik, F.; Engle, K. S.; Bacsa, J.; Sokaras, D.; Kvashnina, K. O.; Li, X.; La Pierre, H. S., Single-

Determinant Ground State in Ce^{4+} Imidophosphorane Complexes. *Inorg. Chem.* **2025**, *64*, 24401-24410.
14. Tateyama, H.; Boggiano, A. C.; Liao, C.; Otte, K. S.; Li, X.; La Pierre, H. S., Tetravalent Cerium Alkyl and Benzyl Complexes. *J. Am. Chem. Soc.* **2024**, *146*, 10268-10273.
15. Yang, Q.; Yu, X.; Lapsheva, E.; Pandey, P.; Smith, P. W.; Gupta, H.; Gau, M. R.; Carroll, P. J.; Minasian, S. G.; Autschbach, J.; Schelter, E. J., Comparison of Ce(iv)/Th(iv)-alkynyl complexes and observation of a *trans*-influence ligand series for Ce(iv). *Chem. Sci.* **2025**, *16*, 16597-16609.
16. Duignan, T. J.; Autschbach, J., Impact of the Kohn–Sham Delocalization Error on the 4f Shell Localization and Population in Lanthanide Complexes. *J. Chem. Theory Comput.* **2016**, *12*, 3109-3121.
17. Xu, W.; Ji, W.-X.; Qiu, Y.-X.; Schwarz, W. H. E.; Wang, S.-G., On structure and bonding of lanthanoid trifluorides LnF_3 (Ln = La to Lu). *Phys. Chem. Chem. Phys.* **2013**, *15*, 7839-7847.
18. Peluzo, B. M. T. C.; Moura, R. T., Jr.; Kraka, E., Correction to "Conformation and Bonding of Lanthanide(III) Trihalides LnX_3 (Ln = La–Lu; X = F, Cl, Br): A Relativistic Local Vibrational Mode Study". *Inorg. Chem.* **2024**, *63*, 24441-24443.
19. Zhang, Y.; Duan, W.; Yang, Y.; Zhao, Z.; Ren, G.; Zhang, N.; Zheng, L.; Chen, J.; Wang, J.; Sun, T., Are 4f-Orbitals Engaged in Covalent Bonding Between Lanthanides and Triphenylphosphine Oxide? An Oxygen K-Edge X-ray Absorption Spectroscopy and Density Functional Theory Study. *Inorg. Chem.* **2024**, *63*, 2597-2605.
20. Merriles, D. M.; London, A.; Tieu, E.; Nielson, C.; Morse, M. D., Probing the Chemical Bond between Lanthanides and Carbon: CeC, PrC, NdC, LuC, and TmC_2. *Inorg. Chem.* **2023**, *62*, 9589-9601.
21. Minasian, S. G.; Batista, E. R.; Booth, C. H.; Clark, D. L.; Keith, J. M.; Kozimor, S. A.; Lukens, W. W.; Martin, R. L.; Shuh, D. K.; Stieber, S. C. E.; Tylisczcak, T.; Wen, X.-d., Quantitative Evidence for Lanthanide-Oxygen Orbital Mixing in CeO_2, PrO_2, and TbO_2. *J. Am. Chem. Soc.* **2017**, *139*, 18052-18064.
22. Vícha, J.; Komorovsky, S.; Repisky, M.; Marek, R.; Straka, M., Relativistic Spin–Orbit Heavy Atom on the Light Atom NMR Chemical Shifts: General Trends Across the Periodic Table Explained. *J. Chem. Theory Comput.* **2018**, *14*, 3025-3039.
23. Straka, M.; Kaupp, M., Calculation of ^{19}F NMR chemical shifts in uranium complexes using density functional theory and pseudopotentials. *Chem. Phys.* **2005**, *311*, 45-56.
24. Vícha, J.; Novotný, J.; Komorovsky, S.; Straka, M.; Kaupp, M.; Marek, R., Relativistic Heavy-Neighbor-Atom Effects on NMR Shifts: Concepts and Trends Across the Periodic Table. *Chem. Rev.* **2020**, *120*, 7065-7103.
25. Novotný, J.; Vícha, J.; Bora, P. L.; Repisky, M.; Straka, M.; Komorovsky, S.; Marek, R., Linking the Character of the Metal–Ligand Bond to the Ligand NMR Shielding in Transition-Metal Complexes: NMR Contributions from Spin–Orbit Coupling. *J. Chem. Theory Comput.* **2017**, *13*, 3586-3601.
26. Vícha, J.; Marek, R.; Straka, M., High-Frequency ^1H NMR Chemical Shifts of Sn^{II} and Pb^{II} Hydrides Induced by Relativistic Effects: Quest for Pb^{II} Hydrides. *Inorg. Chem.* **2016**, *55*, 10302-10309.
27. Kaupp, M.; Malkina, O. L.; Malkin, V. G.; Pyykkö, P., How Do Spin–Orbit-Induced Heavy-Atom Effects on NMR Chemical Shifts Function? Validation of a Simple Analogy to Spin–Spin

Coupling by Density Functional Theory (DFT) Calculations on Some Iodo Compounds. *Chem. Eur. J.* **1998**, *4*, 118-126.
28. Greif, A. H.; Hrobárik, P.; Autschbach, J.; Kaupp, M., Giant spin–orbit effects on ^{1}H and ^{13}C NMR shifts for uranium(vi) complexes revisited: role of the exchange–correlation response kernel, bonding analyses, and new predictions. *Phys. Chem. Chem. Phys.* **2016**, *18*, 30462-30474.
29. Hrobárik, P.; Hrobáriková, V.; Greif, A. H.; Kaupp, M., Giant Spin-Orbit Effects on NMR Shifts in Diamagnetic Actinide Complexes: Guiding the Search of Uranium(VI) Hydride Complexes in the Correct Spectral Range. *Angew. Chem. Int. Ed.* **2012**, *51*, 10884-10888.
30. Kaupp, M., Chapter 9 - Relativistic Effects on NMR Chemical Shifts. In *Theoretical and Computational Chemistry*, Schwerdtfeger, P., Ed. Elsevier: 2004; Vol. 14, pp 552-597.
31. Hayton, T. W.; Autschbach, J., Using NMR Spectroscopy to Evaluate Metal–Ligand Bond Covalency for the f Elements. *Acc. Chem. Res.* **2025**, *58*, 488-498.
32. Du, J.; Seed, J. A.; Berryman, V. E. J.; Kaltsoyannis, N.; Adams, R. W.; Lee, D.; Liddle, S. T., Exceptional uranium(VI)-nitride triple bond covalency from ^{15}N nuclear magnetic resonance spectroscopy and quantum chemical analysis. *Nature Commun.* **2021**, *12*, 5649.
33. Sergentu, D.-C.; Kent, G. T.; Staun, S. L.; Yu, X.; Cho, H.; Autschbach, J.; Hayton, T. W., Probing the Electronic Structure of a Thorium Nitride Complex by Solid-State ^{15}N NMR Spectroscopy. *Inorg. Chem.* **2020**, *59*, 10138-10145.
34. Staun, S. L.; Sergentu, D.-C.; Wu, G.; Autschbach, J.; Hayton, T. W., Use of ^{15}N NMR spectroscopy to probe covalency in a thorium nitride. *Chem. Sci.* **2019**, *10*, 6431-6436.
35. Mullane, K. C.; Hrobárik, P.; Cheisson, T.; Manor, B. C.; Carroll, P. J.; Schelter, E. J., ^{13}C NMR Shifts as an Indicator of U–C Bond Covalency in Uranium(VI) Acetylide Complexes: An Experimental and Computational Study. *Inorg. Chem.* **2019**, *58*, 4152-4163.
36. Ordoñez, O.; Yu, X.; Wu, G.; Autschbach, J.; Hayton, T. W., Assessing the 4f Orbital Participation in the Ln–C Bonds of $[Li(THF)_4][Ln(C_6Cl_5)_4]$ (Ln = La, Ce). *Inorg. Chem.* **2022**, *61*, 15138-15143.
37. Ordoñez, O.; Yu, X.; Wu, G.; Autschbach, J.; Hayton, T. W., Homoleptic Perchlorophenyl "Ate" Complexes of Thorium(IV) and Uranium(IV). *Inorg. Chem.* **2021**, *60*, 12436-12444.
38. Ordoñez, O.; Yu, X.; Wu, G.; Autschbach, J.; Hayton, T. W., Quantifying Actinide–Carbon Bond Covalency in a Uranyl–Aryl Complex Utilizing Solution ^{13}C NMR Spectroscopy. *Inorg. Chem.* **2024**, *63*, 9427-9433.
39. Ordoñez, O.; Yu, X.; Wu, G.; Autschbach, J.; Hayton, T. W., Synthesis and Characterization of Two Uranyl-Aryl "Ate" Complexes. *Chem. Eur. J.* **2021**, *27*, 5885-5889.
40. Kent, G. T.; Yu, X.; Wu, G.; Autschbach, J.; Hayton, T. W., Ring-opening of a thorium cyclopropenyl complex generates a transient thorium-bound carbene. *Chem. Commun.* **2022**, *58*, 6805-6808.
41. Kent, G. T.; Yu, X.; Pauly, C.; Wu, G.; Autschbach, J.; Hayton, T. W., Synthesis of Parent Acetylide and Dicarbide Complexes of Thorium and Uranium and an Examination of Their Electronic Structures. *Inorg. Chem.* **2021**, *60*, 15413-15420.
42. Pedrick, E. A.; Hrobárik, P.; Seaman, L. A.; Wu, G.; Hayton, T. W., Synthesis, structure and bonding of hexaphenyl thorium(iv): observation of a non-octahedral structure. *Chem. Commun.* **2016**, *52*, 689-692.

43. Smiles, D. E.; Wu, G.; Hrobárik, P.; Hayton, T. W., Synthesis, Thermochemistry, Bonding, and ^{13}C NMR Chemical Shift Analysis of a Phosphorano-Stabilized Carbene of Thorium. *Organometallics* **2017**, *36*, 4519-4524.
44. Seaman, L. A.; Hrobárik, P.; Schettini, M. F.; Fortier, S.; Kaupp, M.; Hayton, T. W., A Rare Uranyl(VI)–Alkyl Ate Complex $[Li(DME)_{1.5}]_2[UO_2(CH_2SiMe_3)_4]$ and Its Comparison with a Homoleptic Uranium(VI)–Hexaalkyl. *Angew. Chem. Int. Ed.* **2013**, *52*, 3259-3263.
45. Baker, C. F.; Seed, J. A.; Adams, R. W.; Lee, D.; Liddle, S. T., ^{13}Ccarbene nuclear magnetic resonance chemical shift analysis confirms Ce^{IV}=C double bonding in cerium(iv)–diphosphonioalkylidene complexes. *Chem. Sci.* **2024**, *15*, 238-249.
46. Panetti, G. B.; Sergentu, D.-C.; Gau, M. R.; Carroll, P. J.; Autschbach, J.; Walsh, P. J.; Schelter, E. J., Isolation and characterization of a covalent Ce^{IV}-Aryl complex with an anomalous ^{13}C chemical shift. *Nature Commun.* **2021**, *12*, 1713.
47. Réant, B. L. L.; Berryman, V. E. J.; Basford, A. R.; Nodaraki, L. E.; Wooles, A. J.; Tuna, F.; Kaltsoyannis, N.; Mills, D. P.; Liddle, S. T., ^{29}Si NMR Spectroscopy as a Probe of s- and f-Block Metal(II)–Silanide Bond Covalency. *J. Am. Chem. Soc.* **2021**, *143*, 9813-9824.
48. Du, J.; Hurd, J.; Seed, J. A.; Balázs, G.; Scheer, M.; Adams, R. W.; Lee, D.; Liddle, S. T., ^{31}P Nuclear Magnetic Resonance Spectroscopy as a Probe of Thorium–Phosphorus Bond Covalency: Correlating Phosphorus Chemical Shift to Metal–Phosphorus Bond Order. *J. Am. Chem. Soc.* **2023**, *145*, 21766-21784.
49. Wu, W.; Rehe, D.; Hrobárik, P.; Kornienko, A. Y.; Emge, T. J.; Brennan, J. G., Molecular Thorium Compounds with Dichalcogenide Ligands: Synthesis, Structure, ^{77}Se NMR Study, and Thermolysis. *Inorg. Chem.* **2018**, *57*, 14821-14833.
50. Ringgold, M.; Rehe, D.; Hrobárik, P.; Kornienko, A. Y.; Emge, T. J.; Brennan, J. G., Thorium Cubanes–Synthesis, Solid-State and Solution Structures, Thermolysis, and Chalcogen Exchange Reactions. *Inorg. Chem.* **2018**, *57*, 7129-7141.
51. Nguyen, T. H.; Ausman, S. F.; MacGregor, F.; Wu, G.; Fortier, S.; Hayton, T. W., The Curious Case of $[AnH(NR_2)_3]$ (An = Th, U; R = $SiMe_3$): Two Monomeric Actinide Hydrides Revisited. *Organometallics* **2025**, *44*, 105-114.
52. Nguyen, T. H.; Yu, X.; Wu, G.; Autschbach, J.; Hayton, T. W., Spin-Orbit Effects in a Thallium Borohydride Stabilized by Coordination to Bis(diisopropylamino)Cyclopropenylidene (BAC). *Angew. Chem. Int. Ed.* **2025**, *64*, e202509732.
53. Smiles, D. E.; Wu, G.; Hrobárik, P.; Hayton, T. W., Use of ^{77}Se and ^{125}Te NMR Spectroscopy to Probe Covalency of the Actinide-Chalcogen Bonding in $[Th(E_n)\{N(SiMe_3)_2\}_3]^-$ (E = Se, Te; *n* = 1, 2) and Their Oxo-Uranium(VI) Congeners. *J. Am. Chem. Soc.* **2016**, *138*, 814-825.
54. Vincenzini, B. D.; Schelter, E. J., Organo-cerium(IV) species comprising metallocene-, hydrocarbyl-, carbene-, imido-, and oxo-complexes and related compounds: Emerging insights into bonding, electronic structures, and reactivity trends. *Coord. Chem. Rev.* **2025**, *544*, 216968.
55. Vincenzini, B. D.; Yu, X.; Paloc, S.; Smith, P. W.; Gupta, H.; Pandey, P.; Kent, G. T.; Ordonez, O.; Keller, T.; Gau, M. R.; Bacon, A. M.; Minasian, S. G.; Hayton, T. W.; Autschbach, J.; Schelter, E. J., 4f-orbital covalency enables a single-crystal-to-single-crystal ring-opening isomerization in a Ce^{IV}–cyclopropenyl complex. *Nature Chem.* **2025**, *17*, 961-967.
56. Hazin, P. N.; Huffman, J. C.; Bruno, J. W., Synthetic and structural studies of pentamethylcyclopentadienyl complexes of lanthanum and cerium. *Organometallics* **1987**, *6*, 23-27.

57. Jordi Cirera, E. R., Santiago Alvarez, Continuous Shape Measures as a Stereochemical Tool in Organometallic Chemistry. *Organometallics* **2005**, *24*, 1556-1562.
58. Yu Phan, T. X., Guan-Wen Yang, Kun Jin, Xiao-Bing Lu, Bis(oxazolinyl)phenyl-Ligated Rare-Earth-Metal Complexes: Highly Regioselective Catalysts for *cis*-1,4-Polymerization of Isoprene. *Inorg. Chem.* **2013**, *52*, 2802-2808.
59. Martinez-Arripe, E.; Jean-Baptiste-dit-Dominique, F.; Auffrant, A.; Le Goff, X.-F.; Thuilliez, J.; Nief, F., Synthesis and Characterization of Bidentate Rare-Earth Iminophosphorane *o*-Aryl Complexes and Their Behavior As Catalysts for the Polymerization of 1,3-Butadiene. *Organometallics* **2012**, *31*, 4854-4861.
60. Hogerheide, M. P.; Boersma, J.; Spek, A. L.; van Koten, G., Synthesis of a Bis(cyclopentadienyl)lanthanum Aryl Complex with a Pseudofacially Bound Bis(ortho)-Chelating Aryldiamine Ligand. X-ray Structure of (η^5-C_5H_5)$_2$La(C_6H_3{CH_2NMe_2}$_2$-2,6). *Organometallics* **1996**, *15*, 1505-1507.
61. Maron, L.; Werkema, E. L.; Perrin, L.; Eisenstein, O.; Andersen, R. A., Hydrogen for Fluorine Exchange in C_6F_6 and C_6F_5H by Monomeric [1,3,4-(Me_3C)$_3C_5H_2$]$_2$CeH: Experimental and Computational Studies. *J. Am. Chem. Soc.* **2005**, *127*, 279-292.
62. Pandey, P.; Yu, X.; Panetti, G. B.; Lapsheva, E.; Gau, M. R.; Carroll, P. J.; Autschbach, J.; Schelter, E. J., Synthesis, Electrochemical, and Computational Studies of Organocerium(III) Complexes with Ce–Aryl Sigma Bonds. *Organometallics* **2023**, *42*, 1267-1277.
63. Werkema, E. L.; Andersen, R. A., Fluorine for Hydrogen Exchange in the Hydrofluorobenzene Derivatives $C_6H_xF_{6-x}$, where x = 2, 3, 4 and 5 by Monomeric [1,2,4-(Me_3C)$_3C_5H_2$]$_2$CeH: The Solid State Isomerization of [1,2,4-(Me_3C)$_3C_5H_2$]$_2$Ce(2,3,4,5-C_6HF_4) to [1,2,4-(Me_3C)$_3C_5H_2$]$_2$Ce(2,3,4,6-C_6HF_4). *J. Am. Chem. Soc.* **2008**, *130*, 7153-7165.
64. Ślepokura, K.; Cabreros, T. A.; Muller, G.; Lisowski, J., Sorting Phenomena and Chirality Transfer in Fluoride-Bridged Macrocyclic Rare Earth Complexes. *Inorg. Chem.* **2021**, *60*, 18442-18454.
65. Huang, W.; Diaconescu, P. L., Aromatic C–F Bond Activation by Rare-Earth-Metal Complexes. *Organometallics* **2017**, *36*, 89-96.
66. Wayda, A. L.; Atwood, J. L.; Hunter, W. E., Homoleptic organolanthanoid hydrocarbyls. The synthesis and x-ray crystal structure of tris[*o*-((dimethylamino)methyl)phenyl]lutetium. *Organometallics* **1984**, *3*, 939-941.
67. Johnson, K. R. D.; Hayes, P. G., Synthesis and Reactivity of Dialkyl Lutetium Complexes Supported by a Novel Bis(phosphinimine)carbazole Pincer Ligand. *Organometallics* **2009**, *28*, 6352-6361.
68. Cotton, S. A.; Hart, F. A.; Hursthouse, M. B.; Welch, A. J., Preparation and molecular structure of a σ-bonded lanthanide phenyl. *J. Chem. Soc., Chem. Commun.* **1972**, 1225-1226.
69. Nelsen, M. J.; Girolami, G. S., Synthesis and characterization of zirconium pentafluorophenyl complexes: X-ray crystal structures of [$ZrCl_2(C_6F_5)_4^{2-}$] and [$ZrF_2(C_6F_5)_5^{3-}$]. *J. Organomet. Chem.* **1999**, *585*, 275-284.
70. Decken, A.; Nikiforov, G. B.; Passmore, J., The reaction of TiF_4 with Li($OC(CF_3)_2Ph$): direct synthetic route to the lithium–titanium heterometallic fluoride bridged complex {$Li(THF)_2TiF_3(OC(CF_3)_2Ph)_2$}$_2$ and $Ti(OC(CF_3)_2Ph)_4$ alkoxide. *Dalton Trans.* **2006**, 4328-4334.
71. Clark, C. L.; Lockhart, J. J.; Fanwick, P. E.; Bart, S. C., Synthesis of low-valent uranium fluorides by C–F bond activation. *Chem. Commun.* **2015**, *51*, 14084-14087.

72. Yin, H.; Zabula, A. V.; Schelter, E. J., C–F→Ln/An interactions in synthetic f-element chemistry. *Dalton Trans.* **2016**, *45*, 6313-6323.
73. Deacon, G. B.; Junk, P. C.; Werner, D., Lanthanoid Induced C–F Activation of All Fluorine Atoms of One CF_3 Group. *Eur. J. Inorg. Chem.* **2015**, *2015*, 1484-1489.
74. Guo, Z.; Deacon, G. B.; Junk, P. C., Unexpected C−F activation during redox transmetallation with silver *N*,*N*'-bis(2,6-difluorophenyl)formamidinate. *Z. anorg. allg. Chem.* **2022**, *648*, e202200189.
75. Evans, W. J., The Importance of Questioning Scientific Assumptions: Some Lessons from f Element Chemistry. *Inorg. Chem.* **2007**, *46*, 3435-3449.
76. Falivene, L.; Cao, Z.; Petta, A.; Serra, L.; Poater, A.; Oliva, R.; Scarano, V.; Cavallo, L., Towards the online computer-aided design of catalytic pockets. *Nature Chem.* **2019**, *11*, 872-879.
77. Baerends, E. J.; Aguirre, N. F.; Austin, N. D.; Autschbach, J.; Bickelhaupt, F. M.; Bulo, R.; Cappelli, C.; van Duin, A. C. T.; Egidi, F.; Fonseca Guerra, C.; Förster, A.; Franchini, M.; Goumans, T. P. M.; Heine, T.; Hellström, M.; Jacob, C. R.; Jensen, L.; Krykunov, M.; van Lenthe, E.; Michalak, A.; Mitoraj, M. M.; Neugebauer, J.; Nicu, V. P.; Philipsen, P.; Ramanantoanina, H.; Rüger, R.; Schreckenbach, G.; Stener, M.; Swart, M.; Thijssen, J. M.; Trnka, T.; Visscher, L.; Yakovlev, A.; van Gisbergen, S., The Amsterdam Modeling Suite. *J. Chem. Phys.* **2025**, *162*, 162501.
78. Perdew, J. P.; Burke, K.; Ernzerhof, M., Generalized Gradient Approximation Made Simple. *Phys. Rev. Lett.* **1996**, *77*, 3865-3868.
79. Glendening, E. D.; Landis, C. R.; Weinhold, F., Natural bond orbital methods. *Wiley Interdiscip. Rev. Comput. Mol. Sci.* **2012**, *2*, 1-42.
80. Roos, B. O.; Lindh, R.; Malmqvist, P.-Å.; Veryazov, V.; Widmark, P.-O., New Relativistic ANO Basis Sets for Transition Metal Atoms. *J. Phys. Chem. A* **2005**, *109*, 6575-6579.
81. Clavaguéra, C.; Dognon, J.-P.; Pyykkö, P., Calculated lanthanide contractions for molecular trihalides and fully hydrated ions: The contributions from relativity and 4f-shell hybridization. *Chem. Phys. Lett.* **2006**, *429*, 8-12.
82. Stennett, C. R.; Luevano, M. R.; Queen, J. D.; Nguyen, J. Q.; Moore, W. N. G.; Evans, W. J., Large- and Small-Scale Syntheses of Donor-Free Rare-Earth Triiodides from the Metals and Ammonium Iodide. *Inorganic Chemistry* **2024**, *63*, 16855-16860.
83. Niemeyer, M., 1,2-Dimethoxyethan- und Tetrahydrofuran-Komplexe der Seltenerdmetallnitrate. *Zeitschrift für anorganische und allgemeine Chemie* **2006**, *632*, 1449-1456.
84. Harris, R. K.; Becker, E. D.; De Menezes, S. M.; Granger, P.; Hoffman, R. E.; Zilm, K. W., Further conventions for NMR shielding and chemical shifts (IUPAC Recommendations 2008). *Magn Reson Chem* **2008**, *46*, 582-98.
85. Harris, R. K.; Becker, E. D.; Cabral de Menezes, S. M.; Goodfellow, R.; Granger, P., NMR nomenclature. Nuclear spin properties and conventions for chemical shifts(IUPAC Recommendations 2001). *Pure and Applied Chemistry* **2001**, *73*, 1795-1818.
86. Stalke, D.; Whitmire, K. H., Spectroscopic and structural characterization of 2,4,6-tris(trifluoromethyl)phenyllithium·Et2O: a dimer stabilized by lithium ⋯ fluorine contacts. *Journal of the Chemical Society, Chemical Communications* **1990**, 833-834.

87. van den Broeke, J.; Deelman, B.-J.; van Koten, G., Tetrakis{3,5-bis(perfluorohexyl)phenyl}borate: a highly fluorous anion. *Tetrahedron Letters* **2001**, *42*, 8085-8087.
88. Rausch, M. D.; Tibbetts, F. E.; Gordon, H. B., Perhaloaryl-metal chemistry: II. Pentachlorophenyllithium. *Journal of Organometallic Chemistry* **1966**, *5*, 493-500.
89. Rausch, M. D.; Moser, G. A.; Meade, C. F., The isolation, characterization and synthetic utility of several solid organolithium compounds. *J. Organomet. Chem.* **1973**, *51*, 1-11.
90. Trifonov, A. A.; Weghe, P. V. d.; Collin, J.; Domingos, A.; Santos, I., Synthesis of lanthanide complexes coordinated by an asymmetric cyclopentadienyl ligand. *Journal of Organometallic Chemistry* **1997**, *527*, 225-237.

For Table of Contents Only

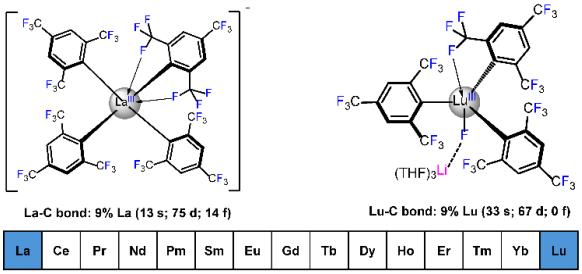

Synopsis

A comparative study of La-aryl and Lu-aryl bonding reveals comparable levels of 5d participation in the Ln-C_{ipso} bonds, as well as comparable levels of spin-orbit deshielding of their C_{ipso} ^{13}C chemical shifts.